JOURNAL OF CATALYSIS 52, 191–205 (1978)

Copper Oxide–Zinc Oxide–Alumina Catalyst: The Structure of a Copper Oxide–Zinc Oxide–Alumina Catalyst for Methanol Synthesis

KIN'YA SHIMOMURA, KIYOSHI OGAWA, MASAAKI OBA, AND YOSHIHIDE KOTERA

National Chemical Laboratory for Industry, 2-19-19, Mita, Meguro-ku, Tokyo, Japan 153

Received August 4, 1976; revised August 3, 1977

Copper oxide–zinc oxide–alumina catalysts for methanol synthesis were prepared by the coprecipitation and kneading methods for comparison of catalytic activity, physical properties, and estimation of the effective surface area by carbon monoxide chemisorption. The coprecipitated catalysts, which are already industrially employed, have higher catalytic activities than the kneaded ones, the optimum chemical composition being around Cu:Zn:Al = 60:35:5 (atom%) in both cases. The total pore volume, the mean pore radius, and the porosity of the coprecipitated catalysts were three to four times larger than those of the kneaded ones. The pore-size distribution ranges from 50 to 5000 Å for the coprecipitated catalysts and from 40 to 10,000 Å for the kneaded ones. The former is equivalent to the copper and zinc oxide values in an individual state, while in the latter the values change in the composite form, with 80- and 20-Å mean particle sizes, respectively. The crystallite size of the composition with a higher catalytic activity after reduction was about 100 Å both for zinc oxide and copper in the coprecipitated catalysts and 170–180 Å for copper and 270–280 Å for zinc oxide in the kneaded ones. From these facts it is proposed that a finely mixed state in the oxidized precursor has its origin during the coprecipitation process. The highest proportion of effective surface area to total surface area in a dense composite was observed over the optimum range of the specific catalytic activity.

INTRODUCTION

Copper oxide–zinc oxide catalysts containing a smaller amount of alumina for the synthesis of methanol (*1*) at lower pressure and temperature are industrially employed with economic and technical advantages (*2*). This catalyst series, which can be preferably prepared by the coprecipitation method, is only empirically outlined in the patent literature except for a few papers dealing with the role of the alumina component (*3*) in the structure, the catalytic activity, and certain aspects of the reaction kinetics (*4*). The present investigation aims at studying the physical properties and the specific catalytic activity as well as the effective surface area of the catalysts, dependent upon the composition, which are generated during the course of catalyst preparation by coprecipitation. The results are compared with those of the corresponding series on catalysts prepared by the kneading method.

EXPERIMENTAL PROCEDURES

Catalyst preparation. The samples studied were prepared by two methods: (A) The precipitate was produced by simultaneously pumping a mixed aqueous solution of the nitrates of copper, zinc, and aluminum in

0021-9517/78/0522-0191$02.00/0

prescribed ratios, in parallel with the precipitant, a sodium carbonate solution, into water contained in the precipitation vessel while stirring at 70°C. The flow rates were separately regulated so as to maintain a pH of 7 ± 0.2 throughout the precipitating process. After washing to remove sodium ions, the precipitate was dried at 110°C and calcined overnight in air at 300°C. The calcined powder was then compressed in the rubber cylinder [15 (i.d.) × 21 (o.d.) × 80 (height) mm] placed in a press apparatus under an oil pressure of 500 kg/cm² to form a cylindrical shape, followed by crushing and sieving to a particle diameter of 1–2 mm. (B) The kneading process was carried out as follows: A mixed aqueous solution of the nitrates of copper and zinc was added to hydrated alumina (*5*) containing 58% water in the bowl of the kneading apparatus. The mixture was kneaded under conditions of gradual heating up to 80°C to yield a viscous paste, in which the nitrates were thermally decomposed in an evaporating dish, and to form a fine powder on further kneading. The sample was then treated in the same way as the coprecipitated series. The composition was determined by means of atomic absorption spectroscopy.

Measurement of catalytic activity. Measurement of catalytic activity was carried out by the use of a conventional flow reactor containing a fixed catalyst bed. The apparatus, as schematically shown in Fig. 1, and operating procedure were similar to those described in a previous paper (*6*), with automatic gas-flow regulating attachments controlled by a differential pressure cell. The reactor, made of an 18-mm-i.d. and 22-mm-o.d. stainless-steel tube, around which manganin wire was wound for internal heating, was placed coaxially in a high-pressure stainless-steel cylinder 60 mm in i.d., 88 mm in o.d., and 450 mm in length. The catalyst (1–2 mm, 5 ml) was supported on a supporting

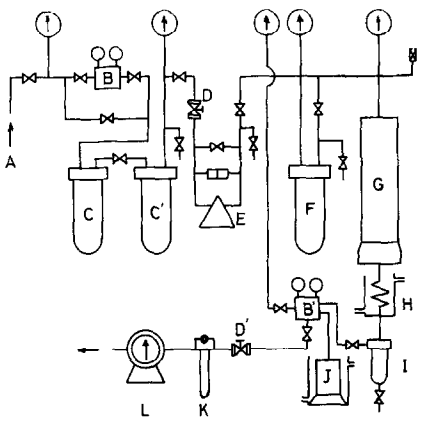

FIG. 1. Diagram of apparatus for testing methanol synthesis catalysts. A, High-pressure gas cylinder; B, B′, secondary and primary pressure regulator; C, C′, high-pressure gas storages (2 liters); D, D′, needle values; E, differential pressure cell; F, gas purifier packed with active charcoal; G, reactor; H, condenser; I, receiver; J, standard pressure vessel; K, flowmeter; and L, gas meter.

plate fixed to the central thermocouple protection tube in the intermediate height range of the reactor. Reduction, with a reactant gas mixture of $2H_2 + 1CO$, was carried out at 300°C at atmospheric pressure for 6 hr in advance of the reaction. Catalytic activity was measured under the following conditions: pressure = 50 kg/cm²; space velocity of the gas supplied from a bomb at STP = 1×10^4 hr^{-1}; and temperature range = 250–370°C. The exit gas and the liquid products from the reactor outlet were analyzed by the usual volumetric method and gas chromatography, respectively.

Measurement of the density, the total pore volume, and the porosity (*7*). The true density, ρ_t, and the particle density, ρ_p, were obtained from the helium-volume and the mercury-volume of catalyst grains, respectively. The total pore volume, V_{po}, was calculated from the difference between both volumes, while the porosity, θ, was derived from the ratio of V_{po} to the mercury volume.

Estimation of the average size of pores and particles. Assuming that the pores were

TABLE 1-1

Catalysts Prepared by the Coprecipitation Method

Catalyst No.	Catalyst composition (Cu/Zn/Al) (atom%)	True density (ρ_t)	Particle density (ρ_p)	Total pore volume (V_{po})
1	20/75/5	4.789	1.181	0.638
2	31.7/63.3/5	4.942	1.192	0.637
3	47.5/47.5/5	5.192	1.205	0.637
4	55/40/5	5.211	1.221	0.627
5	60/35/5	5.235	1.239	0.616
6	75/20/5	5.347	1.332	0.564
7	85/10/5	5.545	1.458	0.506
16	95/0/5	5.734	1.689	0.419
17	0/95/5	4.553	1.163	0.640
8	63.2/36.8/0	—	—	—
9	56.5/33.2/10	—	—	—
10	50.5/29.5/20	—	—	—
11	31.6/18.4/50	—	—	—

TABLE 1-2

Catalysts Prepared by the Kneading Method

Catalyst No.	Catalyst composition (Cu/Zn/Al) (atom%)	True density (ρ_t)	Particle density (ρ_p)	Total pore volume (V_{po})
1-2	20/75/5	5.862	2.950	0.172
3-2	47.5/47.5/5	7.211	3.412	0.154
5-2	60/35/5	6.779	3.247	0.161
7-2	85/10/5	7.379	3.537	0.147
16-2	95/0/5	6.929	3.691	0.127
17-2	0/95/5	6.911	3.755	0.122
9-2	56.5/33.2/10	—	—	—
10-2	50.5/29.5/20	—	—	—
11-2	31.6/18.4/50	—	—	—

cylindrical, the average pore radius, r_{po}, was calculated from V_{po} and the specific surface area, S_{N_2}, and on the assumption of spherical or cubic particles, the average particle radius, R, was calculated from ρ_t and S_{N_2} (*8*).

Measurement of the pore-size distribution. Pore-size distribution was measured by the mercury penetration method with an Aminco 60,000-psi porosimeter and by the nitrogen adsorption method with a Carlo Erba Sorptomatic Series 1800 depending upon the pore-size distributions which are greater or smaller than 300 Å.

Measurement of X-ray diffraction. X-ray diffraction patterns of powdered samples before and after reduction were obtained with a Geigerflex D-3F X-ray diffractometer using nickel-filtered Cu$K\alpha$ radiation. Crystal sizes were determined by calculations employing Scherrer's equation.

Measurement of the surface area by adsorption of nitrogen and carbon monoxide. A specific surface area was determined by applying the BET equation to the adsorption isotherm of nitrogen. The chemisorption of carbon monoxide was chosen as a method for comparing the effective surface area which was estimated by the amount of saturated gas from the adsorption isotherm according to the method described in (*9*).

RESULTS

The chemical composition of the catalysts prepared by both methods are given in Tables 1-1 and 1-2.

Catalytic activity for methanol synthesis. Figure 2 shows a plot of the methanol concentration in the exit gas versus reaction temperature. For the purpose of quantitative comparison of catalytic activities, the rate equation presented by Uchida and Ogino (*6, 10*) was expediently used for the calculation of the rate constant in consideration of the exponential factor as indicated below. Calculated values of the specific rate constant at 300°C, k_{300}, are given in Tables 2-1 and 2-2.

$$k/SV_0 = \int_0^z \frac{\left[\gamma_{CO}\gamma^2_{H_2} \dfrac{4P^3\{1 + (1 - n)z\}\left(\dfrac{n}{2} - z\right)}{(1 + n)^3}\right]^{\alpha} dz}{(1 + 2z)^2\left[\gamma_{CO}\gamma^2_{H_2} \dfrac{4P^3\{1 + (1 - n)z\}\left(\dfrac{n}{2} - z\right)}{(1 + n)^3} - \gamma_{CH_3OH} \cdot Pz/K\right]},$$

TABLE 2-1

Specific Surface Area and Specific Catalytic Activity for the Coprecipitated Catalysts

Catalyst No.	Specific rate constant (k_{300})	Specific surface area (m^2/g)			Specific rate constant ($mol/g \cdot hr \cdot atm^{0.9}$)		
		S_{N_2}	S_{CO}	S_{CO}/S_{N_2}	k/S_{N_2}	k/S_{CO}	$k/S_{CO}/S_{N_2}$
1	8.5×10^{-4}	160	15.0	0.091	5.3×10^{-6}	5.7×10^{-5}	9.4×10^{-3}
2	9.2	181	17.5	0.096	5.1	5.3	9.6
3	9.8	240	22.0	0.091	4.1	4.5	10.8
4	11.4	270	23.0	0.084	4.2	4.9	13.5
5	15.3	272	37.5	0.138	5.6	4.1	11.1
6	10.4	314	30.0	0.096	3.3	3.5	10.9
7	10.6	324	29.4	0.091	3.3	3.6	11.7
16	2.1	337	35.0	0.104	0.6	0.6	2.0
17	1.9	165	9.6	0.058	1.2	2.0	3.2
8	5.0	199	10.1	0.051	2.9	5.6	11.2
9	12.2	266	29.4	0.110	4.6	4.1	11.1
10	10.0	262	28.0	0.107	3.8	3.6	9.4
11	5.6	331	18.4	0.056	1.7	3.1	10.0

which was derived from the rate equation,

$$r = k\{(P_{CO}P^2_{H_2})^{1-\alpha} - P_{CH_3OH}(P_{CO}P^2_{H_2})^{-\alpha}/K\},$$

where SV_0 (in reciprocal hours) is the space velocity based on the feed rate of the synthesis gas, R is the gas constant, γ_i is the activity coefficient of the ith component; P (in atmospheres) is the total pressure of the H_2–CO gas, n is the H_2/CO molecular ratio, z is the mole fraction of methanol in the exit gas, r (moles per hour) is the rate of methanol formation, P_i is the partial pressure of the ith component, K is the equilibrium constant of the reaction, and α is the constant ($0 \leqslant \alpha \leqslant 1$), for which a value of 0.7 was adopted based on the present reaction condition, as also reported in (*3*).

A higher catalytic activity was found in the composition range around Cu:Zn:Al = 60:35:5 (atom%); that is, Cu/Cu + Zn + Al = 0.645, for the coprecipitated series. In catalysts No. 16 and No. 17, containing copper and zinc, respectively, there was greatly reduced, but still distinct, catalytic

TABLE 2-2

Specific Surface Area and Specific Catalytic Activity for the Kneaded Catalysts

Catalyst No.	Specific rate constant (k_{300})	Specific surface area (m^2/g)			Specific rate constant ($mol/g \cdot hr \cdot atm^{0.9}$)		
		S_{N_2}	S_{CO}	S_{CO}/S_{N_2}	k/S_{N_2}	k/S_{CO}	$k/S_{CO}/S_{N_2}$
1-2	4.9×10^{-4}	101	5.3	0.052	4.9×10^{-6}	9.3×10^{-5}	9.5×10^{-3}
3-2	5.1	255	14.5	0.057	2.0	3.5	9.0
5-2	8.9	261	26.3	0.101	3.4	3.4	8.8
7-2	6.1	222	14.0	0.063	2.8	4.4	9.7
16-2	0.6	281	14.0	0.050	0.2	0.4	1.1
17-2	1.4	116	10.5	0.091	1.2	1.3	1.5
9-2	2.8	213	7.0	0.033	1.3	4.0	8.5
10-2	3.5	242	9.2	0.038	1.3	3.3	8.0
11-2	3.1	252	10.4	0.041	1.2	3.0	7.5

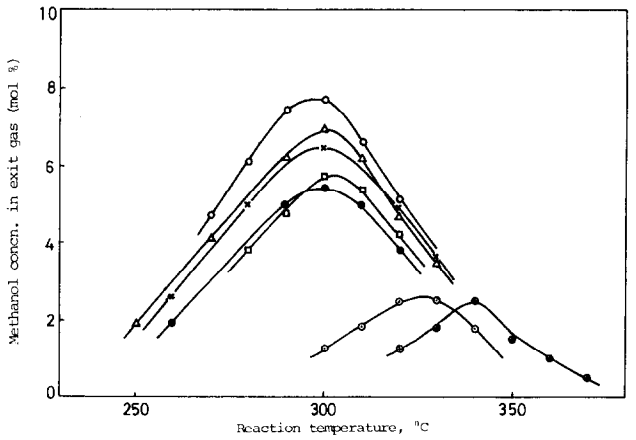

FIG. 2. Catalytic activity for methanol synthesis. —●—, No. 1; —□—, No. 3; —○—, No. 5; —×—, No. 6; —△—, No. 7; —⊙—, No. 16; —⊕—, No. 17.

activity. For the kneaded series lower catalytic activities in the range of the corresponding chemical composition were observed over a higher temperature range.

The gas chromatographic analysis revealed that the liquid reaction product contained small amounts of by-products such as dimethyl ether, methyl formate, methyl propionate, ethyl alcohol, *n*- and isopropyl alcohol, *n*-, s-, and isobutyl alcohol, and a trace amount of water. The total content of these by-products reached 2% for higher activity catalysts and about 4% for catalysts with a content of zinc oxide higher than a ratio of copper/zinc = 1 and with a content of aluminum up to 20%. The latter tended to accompany an an increase of dimethyl ether in the by-products.

Properties of pores and particles. The true density, the particle density, and the total pore volume are listed in Tables 1-1 and 1-2 for both series, respectively. The true density and particle density remain fairly constant as a function of the copper/zinc atomic percentage ratio at fixed aluminum content. Because of the smaller values of the fine porous volumes, the catalysts of the kneaded series have higher density levels than the coprecipitated series. Figure 3 shows the total pore volume and the porosity over the same composition range, while Fig. 4 shows the mean pore radius and the mean particle size. The pore volume for both series is almost constant except for a decrease at very high and low copper contents, especially in the kneaded series, where pore volume is about a quarter of that of the coprecipitated series. The porosity curve is only slightly convex with respect to the composition for the coprecipitated series, which exhibits greater mean radii sizes of pores and particles than the kneaded series. The pore-size distribution and the accumulative pore volume for catalysts No. 5, 16, and 17 of both series are shown in Figs. 5-1 and 6-1 and Figs. 5-2 and 6-2, respectively. In the coprecipitated series the pore-size distribution ranges from 50 to 5000 Å with the maximum around 100 Å both for the composite and for each of the components in an individual state. In the kneaded series, the pore-size distribution ranges widely from 40 to 10,000 Å with the peaks of catalyst No. 5-2 shifted to smaller ranges of radius values than in catalysts No. 16-2 and 17-2. It was observed that the accumulative pore volume tends to increase with an increase in the zinc content and to decrease with increasing copper content. This implies that catalyst

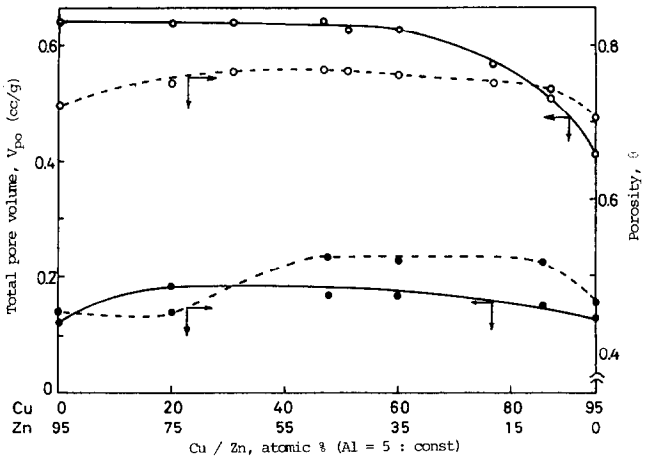

FIG. 3. Total pore volume and porosity plotted against Cu/Zn atomic percentage. ○, coprecipitated; ●, kneaded.

No. 7 is similar to No. 16 and catalyst No. 3 to No. 17 as compared with catalyst No. 5 in the range of optimum composition.

Crystallite sizes before and after reduction. Figures 7-1 and 7-2 show the crystallite sizes of ZnO [100] and CuO [111] for the calcined samples and of ZnO [100] and metallic Cu [111] for the reduced samples, respectively. The X-ray diffraction diagrams gave no indication of any compound formation (*11*) among copper, zinc, and aluminum components in the oxidized state and showed only the complete reduction of copper oxide to metallic copper and some changes in the crystallite size of zinc oxide for the reduced samples. In each of the low concentration ranges of copper and zinc, alternatively, their minor existence was not detected in the X-ray diffraction patterns. For the coprecipitated series before and after reduction, crystallites of zinc oxide, copper oxide, or reduced copper have an identical size on the order of 100 Å in the optimum concentration range. With reduction, samples with a higher concentration zinc oxide showed an

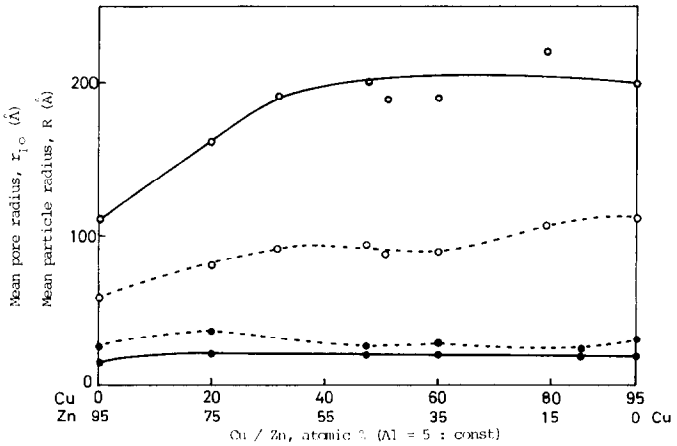

FIG. 4. Mean pore radius and mean particle radius plotted against Cu/Zn atomic percentage. Coprecipitated: —○—, r_{po}; - - -○- - -, R. Kneaded: —●—, r_{po}; - - -●- - -, R.

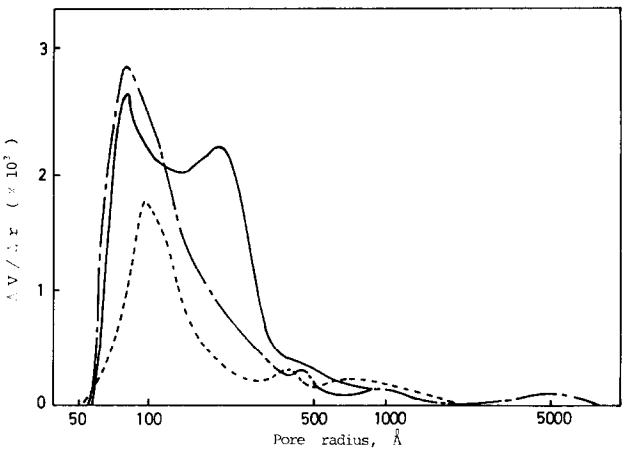

FIG. 5-1. Pore-size distribution of coprecipitated catalysts. ———, No. 5; ------, No. 16; — — —, No. 17.

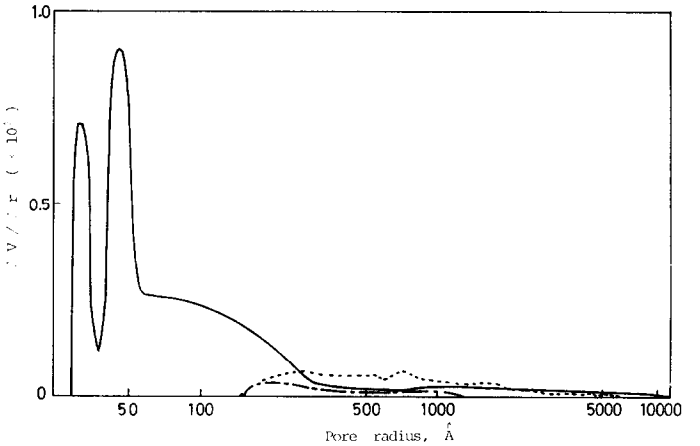

FIG. 5-2. Pore-size distribution of kneaded catalysts. ———, No. 5-2; ------, No. 16-2; — — —, No. 17-2.

apparent growth of crystallites, and larger crystallites of metallic copper were produced when a higher copper concentration was present.

In the optimum composition range, the coexisting crystallites of zinc oxide and metallic copper have the same size as that of the precursory copper oxide. In contrast to this, catalysts of the kneaded series have larger crystallites on the order of 400 Å for zinc oxide and of 160 Å for copper oxide before reduction. With reduction, the crystallite size of zinc oxide decreased considerably but is still twice as large as that of the metallic copper crystallites. This size difference was maintained over the whole range of the catalyst composition except when both sizes became similar with increasing copper content.

Specific surface area estimated by nitrogen and carbon monoxide adsorption. Figure 8-1 demonstrates that after reduction the coprecipitated series showed a remarkable increase in total specific surface area in comparison to the oxidized state with a higher copper content. The kneaded series, with a larger surface area in the oxidized state, showed an increase in specific surface area by reduction in the content range up to the optimum concentration.

This was followed by some decrease when the copper content was increased. From Fig. 8-2, it can be seen that the coprecipitated series exhibits a large increase in the specific surface area with an increasing amount of aluminum in the oxidized state and has a large and unchanging specific surface area in the reduced state for the smaller content range of aluminum of 5-20%, where the part of the catalytically effective component could be regarded as dominant. The kneaded series shows only a minor increase in the specific surface area for the aluminum content below 20 atom%. Aluminum concentrations of less than 50 atom% did not contribute to the development of a highly porous structure. Figures 9-1 and 9-2 show both the measured and estimated effective surface area from the amount of carbon monoxide chemisorbed. This presumptive estimation was made by calculation of the contribution to the effective surface area of the amount of the gas chemisorbed on each of the components, presumably in proportion to the atomic ratios. For both series, the estimated surface area of catalysts No. 1, 3, and 7 and intermediate compositions coincides

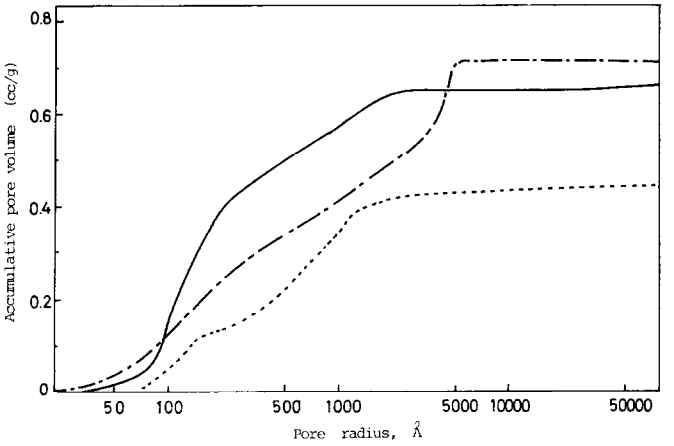

FIG. 6-1. Accumulative pore volume of coprecipitated catalysts. ———, No. 5; - - - - - -, No. 16; — — —, No. 17.

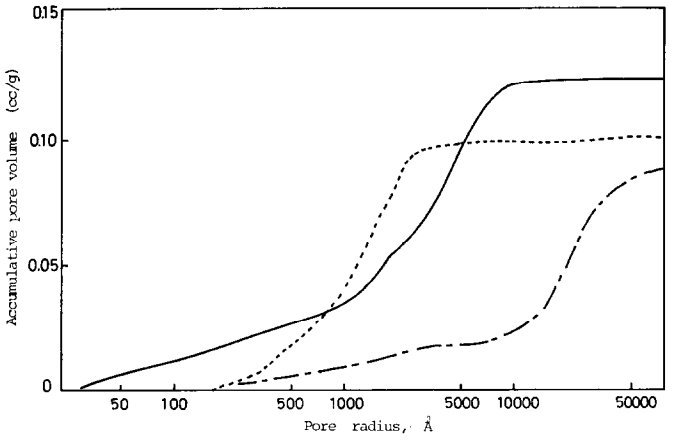

FIG. 6-2. Accumulative pore volume of kneaded catalysts. ———, No. 5-2; - - - - - -, No. 16-2; — — —, No. 17-2.

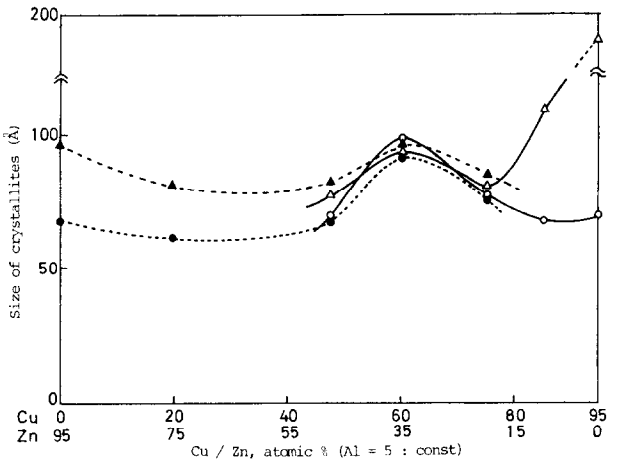

FIG. 7-1. Crystallite sizes of coprecipitated catalysts before and after reduction. —○—, CuO [111]; —△—, Cu [111]; - - -●- - -, ZnO [100] before reduction; - - -▲- - -, ZnO [100] after reduction.

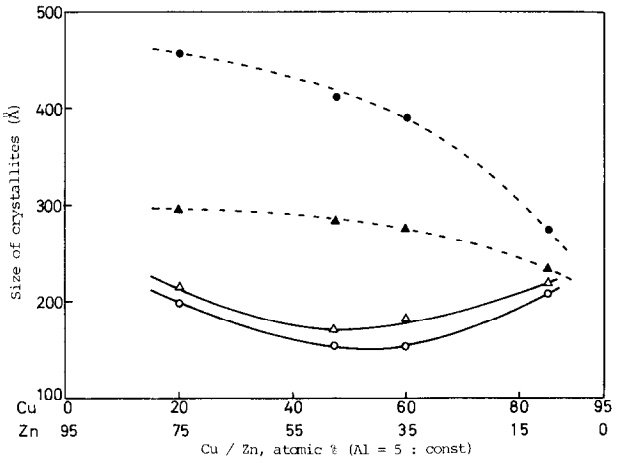

FIG. 7-2. Crystallite sizes of kneaded catalysts before and after reduction. —○—, CuO [111]; —△—, Cu [111]; - - -●- - -, ZnO [100] before reduction; - - -▲- - -, ZnO [100] after reduction.

well with the measured surface area, except when the measured values are higher than the esimation in the catalytically optimum range of composition around catalyst No. 5. Such a characteristic tendency was not observed in the oxidized state, which showed a coincidence over the whole range of the copper/zinc atomic ratio values. The observation suggests that a higher catalytic activity for methanol synthesis in the optimum content range is coupled with a higher effective surface area as estimated by carbon monoxide adsorption. Figure 9-3 shows the dependence of the effective surface area for the reduced samples of both series upon the aluminum content at a fixed atomic ratio of Cu:Zn = 1:0.58, i.e., an atomic percentage of Cu:Zn:Al = 60:35:5 with the highest catalytic activity. For the coprecipitated series, a higher surface area with an apparent maximum around 5 atom% of aluminum decreased with increasing aluminum content, in conjunction with the estimated effective surface area. The kneaded series showed a smaller effective

surface area with the maximum in the same region as the coprecipitated series and a slight increase even above 20 atom% of aluminum. This increasing tendency, which is opposite to a decrease in the copper and zinc contents, shows that these components would be localized inhomogeneously on the alumina surface in the case of the kneaded series of catalysts. This implies that the effective part of added alumina would be blocked with the components, which is experimentally reflected in a rapid deterioration of the catalytic activity as demonstrated in catalyst No. 8 without alumina.

DISCUSSION

Structure of pores and particles. From a comparison between the oxidized states of both series, the catalysts prepared by the coprecipitation method had a much larger total pore volume. This is also apparent in the accumulative pore volume

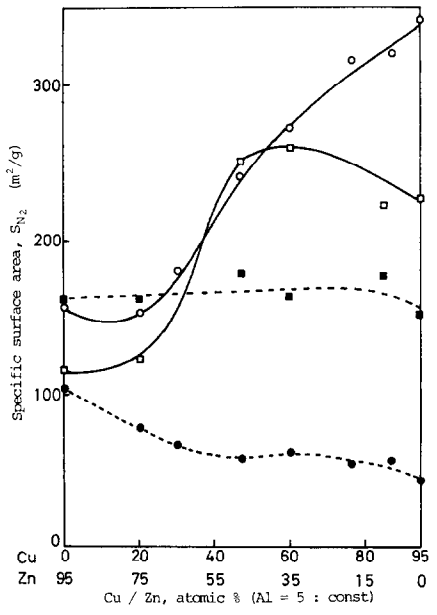

FIG. 8-1. Specific surface as function of Cu/Zn atomic percentage. Coprecipitated: --●--, oxidized; —○—, reduced. Kneaded: —■—, oxidized; —□—, reduced.

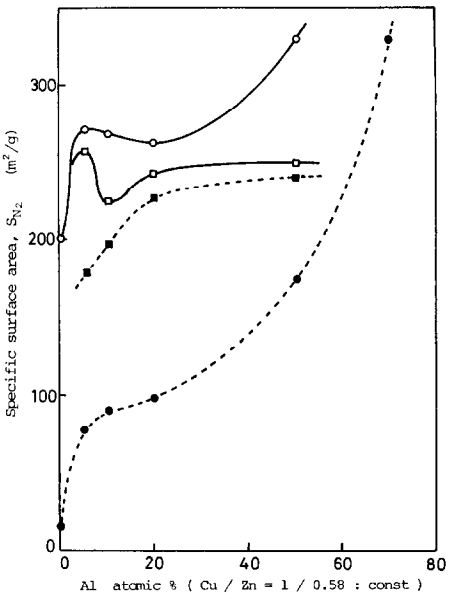

FIG. 8-2. Specific surface as function of Al atomic percentage. Coprecipitated: —●—, oxidized; —○—, reduced. Kneaded: —■—, oxidized; —□—, reduced.

which is several times larger than that of the kneaded series, accompanied with a high porosity. The mean particle radius is in the order of 80 Å for the coprecipitated series and 20 Å for the kneaded series.

These results lead to an interpretation of the structural factors as outlined in the following. The kneaded catalysts can be regarded as an aggregated mass with a small mean pore radius of 20 Å (Fig. 4), which consists of particles with a mean radius of 30 Å, these being conveniently designated as the primary particles (*8*). The aggregate of primary particles has a smaller quantity of the fine pore-size distribution and has a much smaller pore volume in comparison with the coprecipitated series. The larger particles of the order of 80 Å, estimated for the coprecipitated series, fall in the category of the secondary aggregate with a pore radius of a few hundred angstroms. This aggregate constitutes a larger mass with the pore-size distribution of a few thousand

angstroms (Fig. 6-1) to give a large total pore volume. The secondary aggregate disperses on reduction to produce a fairly large surface area.

Crystallite sizes in the coexistent state. The coprecipitated series has a crystallite size of the same order for all components in the optimum content range so as to produce a homogeneous crystallite structure. The kneaded series, with larger crystallites, had a large size difference between copper and zinc oxide resulting in an inhomogeneous structure of mixed crystallites. These observations suggest that the homogeneous structure in the crystallites of the optimum content has its origin during the stage of precipitation so as to produce a fine mixture of precipitates, followed by calcination to precursory oxide. Direct correlation between crystallite sizes which constitute the effective surface and the catalytic activity can not as yet be related to the reaction mechanism; e.g., the kneaded catalyst

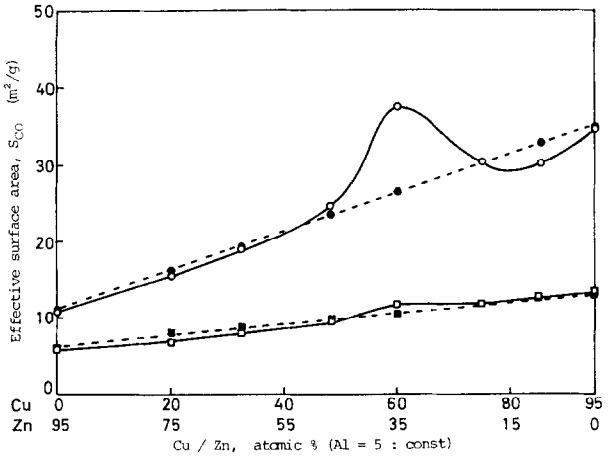

FIG. 9-1. Effective surface area of coprecipitated catalysts before and after reduction plotted against Cu/Zn atomic percentage. Reduced: —○—, measured; —●—, estimated. Oxidized: —□—, measured; —■—, estimated.

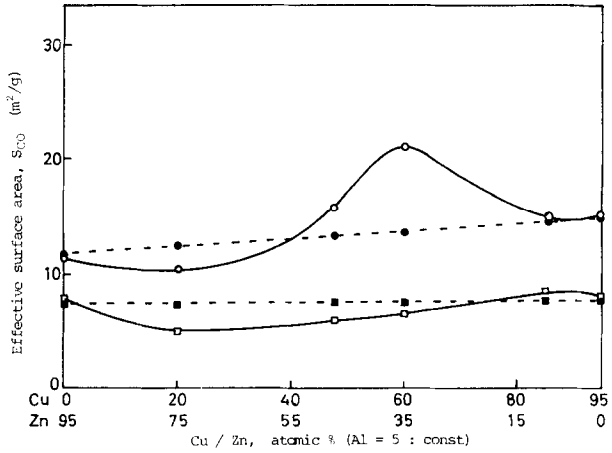

FIG. 9-2. Effective surface area of kneaded catalysts before and after reduction plotted against Cu/Zn atomic percentage. Reduced: —○—, measured; —●—, estimated. Oxidized: —□—, measured; —■—, estimated.

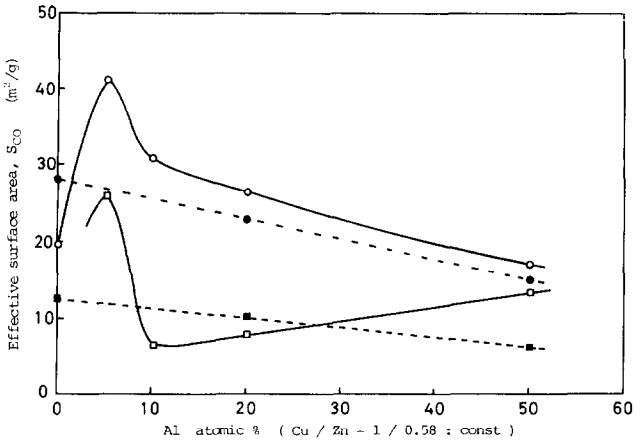

FIG. 9-3. Effective surface area of coprecipitated and kneaded catalysts after reduction plotted against Al atomic percentage. Coprecipitated: —○—, measured; —●—, estimated. Kneaded: —□—, measured; —■—, estimated.

series had a higher catalytic activity in the case of the carbon monoxide-shift conversion (*12*).

Surface area estimated by BET method and by carbon monoxide adsorption. The coprecipitated catalysts with a surface area of 60–70 m^2/g in the oxidized state had a large area increase up to 270–280 m^2/g within the optimum content range on reduction. The higher the copper content the larger the extent of surface area increment. This tendency is correlated to the dominant occupation of the before-mentioned secondary particles with an increase of copper content.

Structural properties of higher concentrations of reduced copper containing only a small amount of alumina were extremely variable, even under conditions of controlled reduction so that strict reproducibility of the experimental results were difficult to obtain. For the kneaded series with a higher copper content, copper particles with an inhomogeneous structure

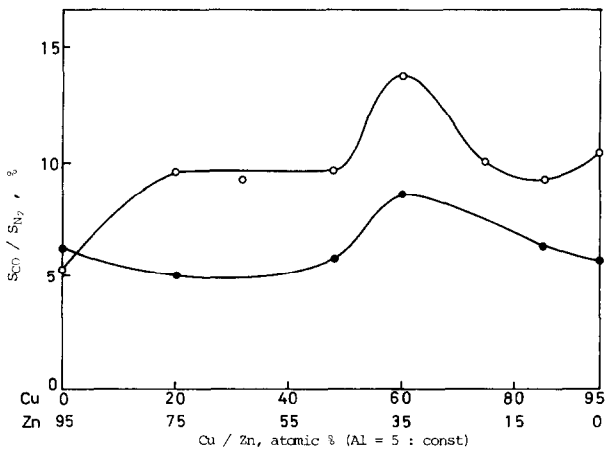

FIG. 10. Ratio of the effective specific surface area to the total specific surface area. —○—, coprecipitated; —●—, kneaded.

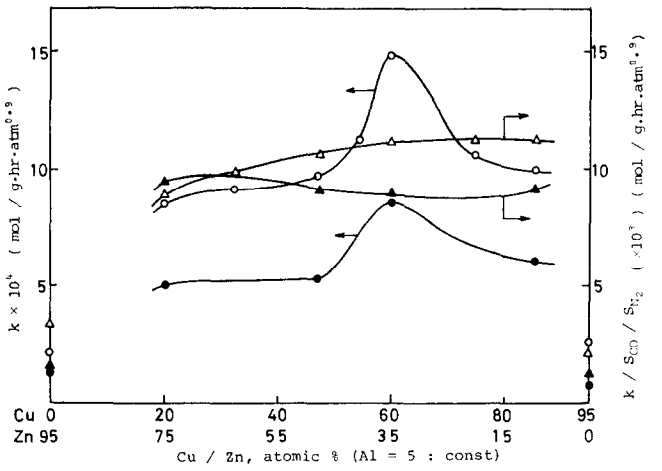

FIG. 11-1. Specific rate constant for methanol synthesis as function of Cu/Zn atomic percentage. —○—, —△—, coprecipitated; —●—, —▲—, kneaded.

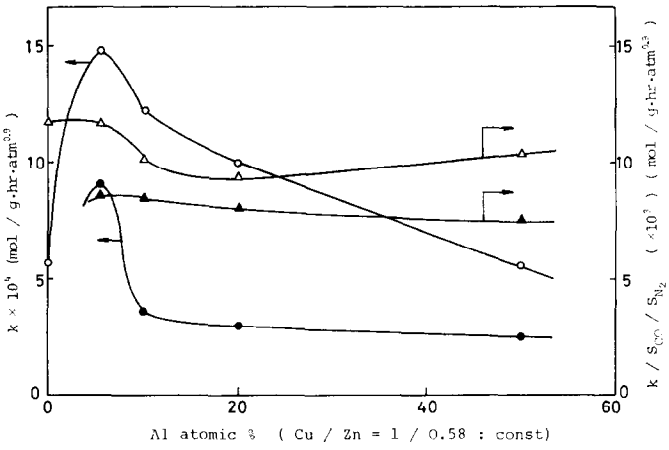

FIG. 11-2. Specific rate constant for methanol synthesis as function of Al atomic percentage. —○—, —△—, coprecipitated; —●—, —▲—, kneaded.

result in a structural inconstancy depending upon the degree of aggregation and crystallite growth.

The kneaded series in the oxidized state had a specific surface area of 170 m^3/g and had a surface area in the order of 270 m^2/g after reduction which is similar to the coprecipitated series within the optimum content range. This was followed by a further decrease in surface area with an increase in copper content. The extent of increment of the specific surface area on reduction is larger for the coprecipitated series which possibly consists of the secondary particles in the oxidized state as compared with the kneaded series which consists only of primary particles. The structural behavior of copper and zinc components, when they coexist, is conveniently comparable to the catalyst samples prepared by the same kneading method (*8*), in which zinc oxide powder was kneaded with a copper hydroxide cake into a paste mixture. In this case the primary particles of copper were found to be attached to the surface of the zinc

oxide particle which retained the original shape and size throughout the thermal treatment process.

In the present catalysts, especially for those of the coprecipitated series, both the copper and zinc components took part in the development of the effective surface structure during thermal treatment, as shown, for instance, by their crystal growth. With reduction the specific surface area showed a greater increase for the coprecipitated series in the optimum content range and a lesser increase and a rough constancy below 50 atom% of aluminum for the kneaded series. In the latter case alumina would have a negligible effect on the growth of surface area because of its low miscibility and dispersity. This result suggests that a supporting material which serves as a dispersing agent and/or thermal stabilizer should be coexistent during precipitation and that it should be coprecipitated rather than added as a suspension or in a stable form like hydrated oxide. The higher effective surface area measured by carbon monoxide adsorption was observed for both series in the catalytically optimum content range. The proportion of chemisorbed carbon monoxide that can be attributed to the metallic part and to the other effective part has not been determined because of some uncertain factors related to the selective adsorption during the experimental conditions. Each of the components, copper and zinc oxide, showed a much lesser but nevertheless clear catalytic activity in their individual states. The nature of the active sites as determined from the difference of carbon monoxide chemisorption between the oxidized and reduced states cannot yet be satisfactorily explained although it is clear that metallic copper produced by reduction plays a dominant role in the reduced catalysts (*3*, *13*).

Specific catalytic activity for methanol synthesis. As shown in Fig. 10, a higher ratio of effective surface area, S_{CO}, to specific surface area, S_{N_2}, was observed in the optimum content range of the ratio of copper/zinc which compositely constitute a higher density of active sites. Figures 11-1 and 11-2 demonstrate the specific rate constant based on the unit weight and ratio of S_{CO}/S_{N_2} plotted against catalyst composition. The specific activity, $K/S_{CO}/S_{N_2}$, had a fairly constant level over a wide range of the composition, around 1.1×10^{-2} for the coprecipitated catalysts and 9×10^{-3} mol/g·hr·atm$^{0.9}$ for the kneaded catalysts, the latter having a less dense distribution of catalytically active sites.

The specific rate constant, assumed on the basis of the total specific surface area, S_{N_2}, and on the effective surface area, S_{CO}, showed no higher range in catalytic activity as a function of the chemical composition. It had a fairly constant level and showed slight tendency to decrease with an increase in the copper/zinc ratio (Tables 2-1 and 2-2).

These results suggest that a higher catalytic activity requires that the catalyst components coexist in a finely divided state of a dense composite so as to constitute a higher proportion of the effective surface area compared with the total surface area.

Further study is needed to clarify the active sites in the effective surface area, taking the reaction mechanism into account, the kinds of reactant gas, hydrogen, carbon monoxide and/or carbon dioxide, to be adsorbed (*13–19*), the conditions of individual or concurrent adsorption, and the heat of selective adsorption.

REFERENCES

1. U. S. Pat. 1,159,035, 1,296,212; Belg. Pat. 685,706, 743,652; F. Pat. 1,489,682; D. Pat. 2,302,658, 2,320,192; Japan. Pat. S45-16682, S49-42240.
2. Miyashita, Y., *Petrol. Petrochem.* **13**, 76 (1969); Bolton, D. H., *Chem. Ing. Tech.* **41**, 129

(1969); Bolton, D. H., and Hanson, D., *Chem. Eng.* **154**, Sept. 22, 1969.

3. Mitsushima, H., and Ishizuka, A., *Kogyo Kagaku Zasshi* **72**, 2360 (1969).
4. Atroshchenko, V. I., Leonov, V. E., and Karavaev, M. M., *Kinet. Katal.* **12**, 160 (1971); Leonov, V. E., Karavaev, M. M., Tsybina, E. N., and Petrishcheva, G. C., *Kinet. Katal.* **14**, 970 (1974).
5. Yamadaya, S., Kinoshita, T., Shimomura, K., and Uchida, H., *Kogyo Kagaku Zasshi* **73**, 849 (1970).
6. Oba, M., Ogino, Y., and Uchida, H., *Rep. Govt. Chem. Ind. Res. Inst. Tokyo* **60**, 121 (1965).
7. Orr, Jr., C., and DallaValle, J. M., "Fine Particle Measurement," p. 257. Macmillan, New York, 1959; Otsuka, A., *in* "Funtai Bussei Zusetsu" (Research Association for Powder Technology, Ed.), pp. 99 and 115. Sangyo Gijutsu Center, Tokyo, 1975.
8. Uchida, H., Oba, M., Isogai, N., and Hasegawa, T., *Bull. Chem. Soc. Japan* **41**, 479 (1968).
9. Sinfelt, J. H., Taylor, W. F., and Yates, D. J. C., *J. Phys. Chem.* **69**, 95 (1965); Araki, M., and Kotera, Y., *Bull. Japan. Petrol. Inst.* **15**, 45 (1973).
10. Uchida, H., and Ogino, Y., *Bull. Chem. Soc. Japan* **31**, 45 (1958).
11. van Herwijnen, T., and de Jong, W. A., *J. Catal.* **34**, 209 (1974); Japan. Pat. S49-42240, S47-10119.
12. Uchida, H., Isogai, N., Oba, M., and Hasegawa, T., *Bull. Chem. Soc. Japan* **40**, 1981 (1967).
13. Terao, I., Uda, A., and Kuraishi, M., *Shokubai* **8**, 279 (1966).
14. Nagarjunan, T. S., Sastri, M. V. C., and Kuriacose, J. C., *J. Catal.* **2**, 223 (1963).
15. Tsuchiya, S., and Shiba, T., *Bull. Chem. Soc. Japan* **38**, 1726 (1965); *Bull. Chem. Soc. Japan* **40**, 1086 (1967); *Bull. Chem. Soc. Japan* **41**, 573 (1968).
16. Aharoni, C., and Tompkins, F. C., *Trans. Faraday Soc.* **66**, 434 (1970); Aharoni, C., and Starer, H., *Canad. J. Chem.* **52**, 4044 (1974).
17. Korenevskaya, F. V., Pershina, L. M., and Rozovskii, A. Ya., *Kinet. Katal.* **12**, 1358 (1971); *Kinet. Katal.* **17**, 198 (1976).
18. Gerasimova, G. F., Keier, N. P., and Isaenko, L. I., *Kinet. Katal.* **14**, 1239 (1973).
19. Rudnitskii, L. A., Maksimova, N. P., and Alekseev, A. M., *Kinet. Katal.* **14**, 1505 (1973).